Localized structures in chaotic patterns: From disorder to ordering

M. Le Berre, A. S. Patrascu, E. Ressayre, and A. Tallet
Laboratoire de Photophysique Moléculaire du CNRS, 91405, Orsay, France
(Received 19 March 1997)

Two-dimensional (2D) ''chaotic'' localized structures are observed in the transverse profile of light with a delay model of a ring cavity with strongly dispersive two-level atoms. Near nascent optical bistability, the 2D homogeneous solution undergoes a subcritical transition to a spatiotemporal chaos. The inhomogeneous pattern coexisting with the homogeneous solution is filled with large-intensity peaks, oscillating with time. In the subcritical domain, localized structures are observed, with isolated peaks more stable and more coherent than the ones in the filled structure. The order is easily recovered by a filtering procedure that reduces the wave-vector bandwidth. [S1050-2947(97)10409-7]

PACS number(s): 42.65.Pc, 42.60.Mi

I. INTRODUCTION

Two-dimensional localized structures, also called Ising patterns or bubbles [1], are observed in hydrodynamics [2] and chemistry [3,4], and also in optics [5–8]. In all cases the localized structures occur when two different stable states coexist in a certain range of control parameters. The simplest localized structures are patterns showing an interface between two stable homogeneous states (with constant amplitude). Other localized structures result from the coexistence of stable homogeneous and inhomogeneous solutions, the inhomogeneous solution being generally stripes [5] or hexagons [5–7]. In these cases the localized structures appear as peaks (or holes) emerging on a flat background. An N-peak structure can be produced by adding N Gaussians to the flat incident profile, and allowing the system to evolve to a stationary state. In an N-peak structure, the maxima have the same value as in the periodic (stripe or hexagonal) one, and the background level is equal to that of the nontrivial plane-wave solution. These localized structures are thus a signature of the coexistence of homogeneous and nonhomogeneous states.

Here we report (Sec. II) a numerical observation of ''chaotic'' localized structures resulting from the coexistence of a stable plane-wave solution and a weakly chaotic pattern, with disorder and time-varying intensity peaks; consequently the peaks in localized structures are also set with various intensity values. The equations are those of a delay model of a ring cavity, with saturable two-level atoms having null or finite decay time [Eqs. (1)], which display chaotic solutions in the domain of parameters studied here, corresponding to a nascent optical bistability in the dispersive limit. While the delay model was shown [9–11] to be equivalent to the Lugiato and Lefever (LL) mean-field model for an instantaneous Kerr medium [12] in our previous papers relative to stationary patterns with small intensity, it is no longer equivalent in the present study dealing with high-intensity patterns.

It is known [13] that, close to nascent optical bistability, the process of destabilization of the homogeneous solution is not reducible to a Turing instability, with a single critical wave number K_{th}. Actually the whole band of wave numbers, $0 \leqslant K \leqslant$ few K_{th}, may be involved in the pattern-forming process, and their interplay gives rise to the chaotic solution. We thus show that localized solutions occur not only for envelope equations which are valid close to the onset of instability, but also for a system of two coupled equations valid in the dynamical regime far above the threshold. Finally, a very simple procedure is suggested to change a chaotic solution into an ordered one. A low-frequency filter is set inside the cavity, reducing the spatial bandwidth of the electric field at the input of the cell (Sec. IV). This procedure decreases the peak intensity and stabilizes the spatiotemporal behavior of the solution. A narrow-band filter changes the chaos into hexagons, while a broader filter transparent for the K and $\sqrt{2}K$ components leads to a square pattern. The role of the filter is then to control the chaos in the sense that these two stable periodic patterns are observed far from optical bistability in the delay model. Recall that the regular pattern for a tuned cavity is hexagonal on the focusing side of the resonance [7,9], and squares are formed in the defocusing side, due to the biconical emission of two modes with magic wave-number ratio $\sqrt{2}$ [11]. The changeover from chaos to hexagons is illustrated analytically by investigating the amplitude equations, which receives finite solution by removing nonlinear terms corresponding to the filter operation.

II. LOCALIZED STRUCTURES

The model for the passive ring cavity numerically investigated in this paper was stated in Refs. [9,10]. It generalizes the Ikeda equations [14], including diffraction in the free space of the cavity. With the notation of Ref. [11], the two equations for the electric field E and the atomic population inversion ϕ are

$$E(t+d,\mathbf{x}) = E_0(\mathbf{x}) + \rho \exp\left[i\frac{L}{2k}\nabla_T^2 \right] E(t,\mathbf{x}) \times e^{\alpha\ell(1+i\eta\Delta)\phi/2 - i\eta\theta_{\mathrm{cav}}}, \tag{1a}$$

$$T_1 \frac{d\phi}{dt} = -(\phi+1) - \frac{e^{\alpha\ell\phi}-1}{\alpha\ell}|E|^2. \tag{1b}$$

In Eqs. (1) the diffraction is decoupled from the nonlinearity in the medium. Thus the light beam simply undergoes

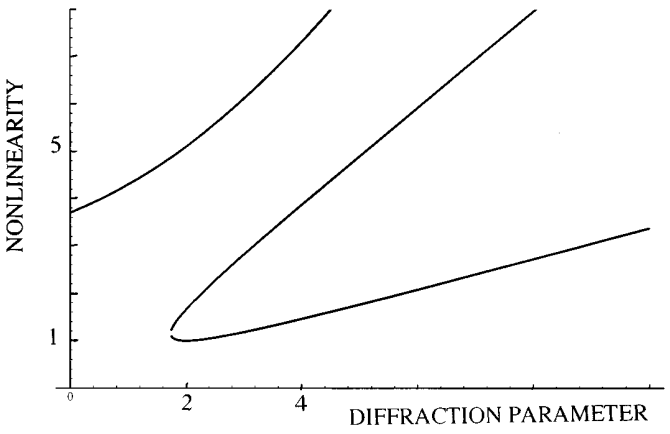

FIG. 1. Static (lower curve) and dynamical (upper curve, in solid line) linear instability boundaries for Eqs. (1) and (2). Parameters are as in Eq. (2). The ''nonlinearity'' $a\alpha\ell\Delta\ I/2\ (a=9)$ is drawn vs the ''diffraction parameter'' $10[(K^2L/2k)+\theta]$, with this scaling the static boundary fits very well the marginal stability curve of Eq. (5) drawn in Fig. 8.

a nonlinear absorption and has a nonlinear phase, inside the cell, proportional to the atomic population inversion. Equations (1) were justified within a given range of parameters, in the sense that the solutions display the same linear threshold characteristics as the full set of Maxwell-Bloch equations [9,10].

In the case treated here of the focusing side of the resonance, $\eta=1$, and for the parameter values

$$\rho=0.95,\ \ \alpha\ell=0.1,\ \ \alpha\ell\Delta=8\pi,\ \ T_1=d, \tag{2}$$

the agreement between the delay model [Eqs. (1)] and the full set of Maxwell-Bloch equations is very good, since the first (static), and also the second (dynamical) linear boundaries (see Fig. 1) coincide, when the radiative lifetime T_1 is of order of the round-trip time d, or much smaller, and for a total diffraction path L equal to the cell length ℓ, or much larger than ℓ [9,10].

Relations (2) mean that we focus on a high finesse cavity containing a strongly dispersive and weakly absorptive medium. The parameter values in Eq. (2) are those of the feedback mirror experiment [17], with a sodium cell containing a high buffer gas pressure. In the ring cavity case, we have shown [10] that one can neglect the polarization dephasing time T_2 for $T_2\leqslant 0.1T_1$, which is different from the case of the feedback mirror [18], where the $2d$ oscillation could not be reproduced if one performs an adiabatic elimination of the polarization. We numerically investigated the cases $T_1=d$ and $T_1=0$, because in the feedback mirror experiment, the turning spots were observed for a ''large'' round-trip time $d\geqslant T_1$. The numerical results presented here concern the case $T_1=d$, because it should be easier to realize experimentally, but very similar results are obtained in the case of an instantaneous atomic response, $T_1=0$.

Let us recall that the linear stability analysis of Eqs. (1) and (2) predicts multiconical emission. The lowest thresholds correspond to the static instability, with coordinates $(I_{\rm th},\Theta_{{\rm th},n})$ given by the relations [10]

$$\tfrac{1}{2}\alpha\ell\Delta|E_{\rm th}|^2=0.1, \tag{3}$$

$$\frac{L}{2k}K_{\rm th}^2+\theta_{\rm cav}=\Theta_{{\rm th},n}=0.2+2n\pi. \tag{4}$$

Above the static instability frontier, there is a second set of curves corresponding to a dynamical instability, with minima twice as high, that is also periodic with respect to the diffraction parameter Θ. In this paper we describe the patterns obtained on the vicinity of nascent optical bistability, which occurs at $\theta_{\rm cav,ob}=0.17$. For that purpose we are only concerned with boundaries close to the optical axis $(K=0)$ shown in Fig. 1. Along the dynamical curve, the threshold T/d period increases from 10 to 40 [9,10]. For $T_1=0$, the dynamical frontier is located far above irrelevant for our study.

The 2D patterns discussed here were obtained for the case $\theta_{\rm cav}=0.16$. The numerical code was described in Refs. [9,10] and the results are obtained by taking 128×128 and 256×256 grids for the transverse variables (x,y), and ten time steps in one round-trip time d. A random noise of relative amplitude 10^{-3}–10^{-4} is added to the input field E_0, the boundary conditions are periodic, and the transverse grid is orthogonal and 1% asymmetrical. With the parameter values given in Eq. (2), the threshold corresponds to $E_0^{\rm th}=0.01$, $I_{\rm th}=|E_{\rm th}|^2=0.0081$.

Just above the linear threshold, the solution of Eqs. (1) is chaotic, both in space and time. For an input field $E_0^{(1)}=0.0105$, two examples of chaotic patterns corresponding to two different initial conditions are shown in Figs. 2(a)–2(c), which display the transverse intensity $I(x,y)$ at a given sampling time t much larger than the transient. The moonlike pattern in Fig. 2(a) has peaks and craters with a chaotic on-axis intensity [Fig. 2(b)]. The other pattern displays many peaks of very different heights, and a weakly chaotic on-axis intensity [Figs. 2(c) and 2(d)]. The maximum intensity is about 11 and 15 times the critical one $I_{\rm th}$, respectively. In both cases the intensity widely overpasses the dynamical threshold. The pattern with peaks in Fig. 2(c) seems less chaotic than the moonlike one; indeed, one can see some peaks aligned along directions making angles of 120° that seems reminiscent of the hexagonal order. Actually, however, this order is only local, as illustrated in the spatial spectrum in Fig. 2(e), which contains components on a wide annulus corresponding nearly to the range $1.4\leqslant K/K_{\rm th}\leqslant 3$. In summary, the chaotic solution in Fig. 2(c), displays a large dispersion of the peak intensities, a disorder in the peak alignment, and a broadband wave-number spectrum. Let us now describe the inhomogeneous solutions obtained below the linear threshold, by decreasing the control parameter from $E_0^{\rm th}=0.01$ to $E_0^{\rm sc}=0.0093$, and starting from the chaotic pattern with disordered peaks as initial condition Fig. 2(c).

(1) In the sequence obtained by slowly decreasing the control parameter (with a gap $\delta E_0=0.01E_0^{(1)}$), all the patterns have the same number of peaks, located at the same place, (Fig. 3), and are very intense. The maximum intensity $I_{\rm max}$ is always of order-11 times the plane-wave value $I_s(E_0)$. As E_0 decreases, the structure stabilizes, in the sense that the peak intensities become constant with respect to time, and spatially more uniform. More precisely, the con-

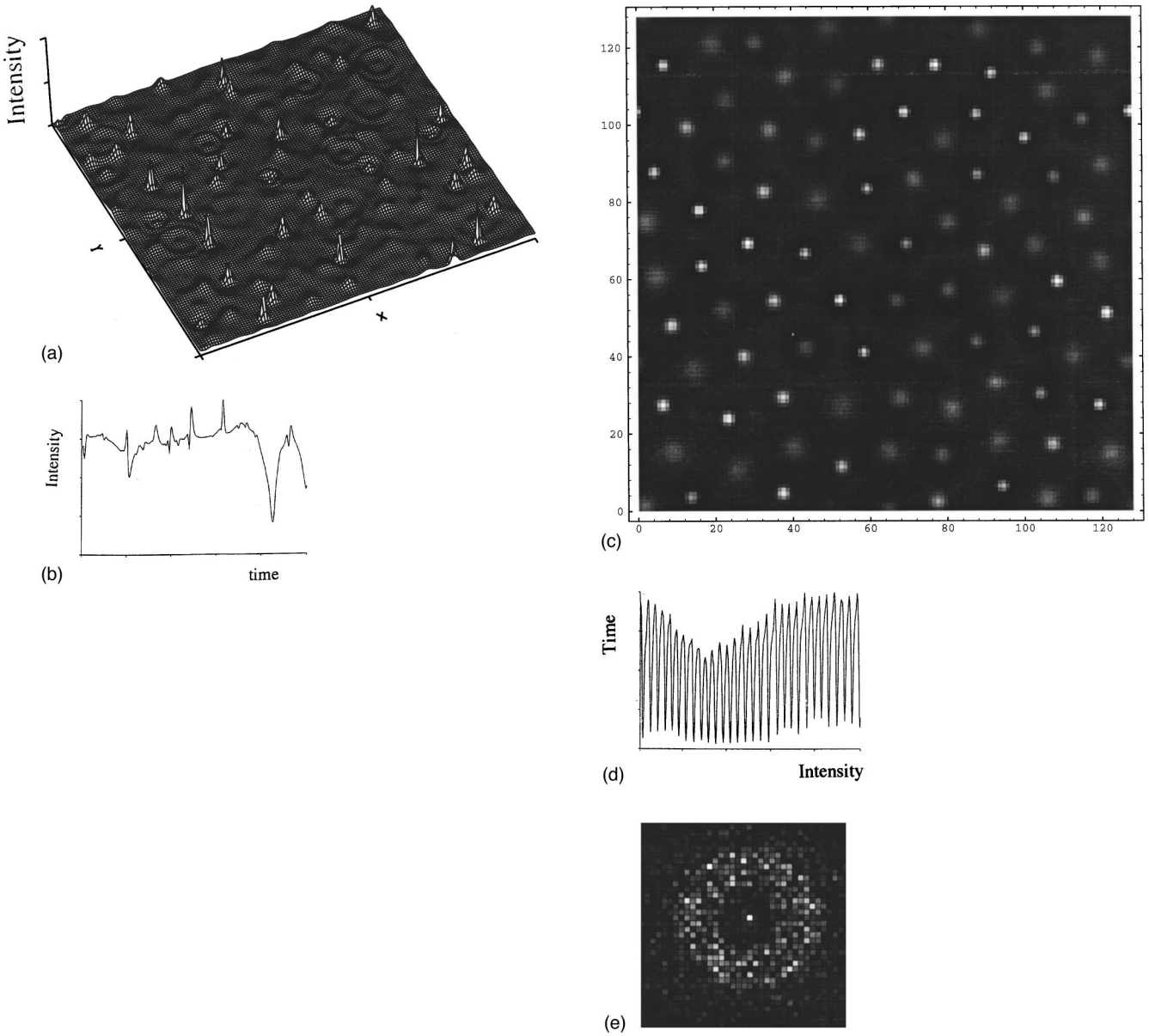

FIG. 2. (a) 3D graph of the intensity $I(x,y,t)=|E(x,y,t)|^2$ at the cell input, in the transverse plane (x,y) for the chaotic solution of Eqs. (1), at a given time t after the transient, for input field amplitude $E_0=0.0105$. (b) Time trace $I(0,0,t)$ during a time interval equal to $500d$, or $50\tau_{\rm ph}$ (the photon lifetime in the cavity $\tau_{\rm ph}$ is equal to ten times the round-trip time d, $\tau_{\rm ph}=d/(1-\rho')$. (c) and (d) Density plot and time trace of the intensity as in (a) and (b) with different initial conditions. (e) Density plot of the far-field intensity, $I(K_x,K_y)$or spatial Fourier spectrum for the chaotic solution in (c).

trast between the maxima $\delta I=2(I_{\rm max}-I_{\rm min})/(I_{\rm max}+I_{\rm min})$ decreases from 50% to 10%. Just below threshold, at $E_0=0.01$, a local peak time trace is weakly chaotic, while, at $I_0=0.0098$, the time trace is quasiperiodic, with a large period $T\approx 51d$, and a modulation at a period about $560d$. At $E_0=0.0097$, the time trace becomes constant. The peaks disappear at $E_0^{\rm sc}=0.0093$ leading to the homogeneous solution.

(2) In the sequence obtained by decreasing the control parameter with a larger value of the decrement δE_0, the solutions exhibit localized structures, with a smaller number of peaks. In some domain of the transverse plane, the intensity is equal to the plane-wave solution I_s, while in other domains the chaotic solution with peaks still remains. The area of the homogeneous solution becomes larger as δE_0 increases. For example, the 35- and three-peak patterns shown in Figs. 5(a) and 6(a), are the localized structures obtained at $E_0=0.0097$, from initial patterns formed at 5% and 11.5% above threshold, respectively.

The 35- and three-peak structures are obtained in the whole domain $(E_0^{\rm th};\ E_0^{\rm sc})$ by decreasing the control parameter down to $E_0^{\rm sc}$, and by slowly varying the control parameter, as in the case of the filled pattern. In this procedure an N-peak pattern is obtained by *seeding* the homogeneous profile with N peaks with approximate height and width, as described in Refs. [5–8].

The spatiotemporal properties of the localized structures can be compared with those of the pattern filled with peaks (obtained for the same value of E_0), in the whole sequence $(E_0^{\rm th};\ E_0^{\rm sc})$. The heights of the peaks are qualitatively the same, but their temporal evolution differs. For example, at

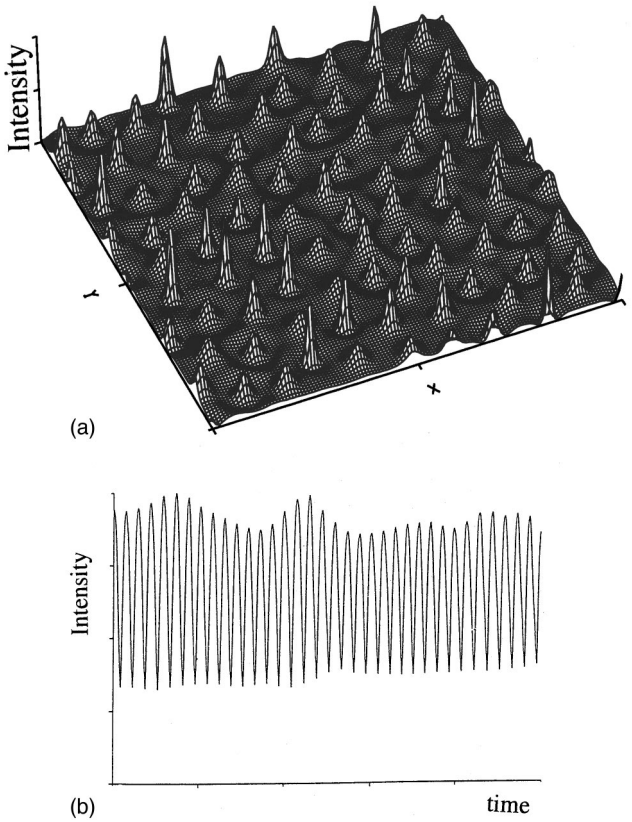

FIG. 3. (a) 3D graph of the chaotic intensity $I(x,y)$ for the ''filled'' structure, obtained just below the threshold for $E_0=0.01$. (b) The on-axis intensity $I(0,0,t)$ during $1800d$.

$E_0=0.0098$, the 35 and three-peak structures are stable, while the time trace for the filled pattern is quasiperiodic (Figs. 4). For $E_0=0.01$ the time trace for a particular peak of the localized structure is periodic [Fig. 5(b)], but weakly chaotic for the filled pattern [Fib. 3(b)]. *Thus the presence of homogeneous domains seems to stabilize the temporal behavior of the structure.*

The coherence properties of peaks differ in the dynamical regime. In the filled structure, the intensity time traces for three distant maxima show various regimes [Figs. 4(a)–4(c)], the phase relations between the three peaks changing with time. During a certain time interval two given peaks oscillate coherently, but suddenly the relative phase changes. Conversely, in the case of the three-peak structure, the peaks oscillate in phase with time traces in exact coincidence [Fig. 6(b)]. Consequently *the large intrapeak distance favors the coherent properties of the light.*

While in the three-peak pattern the peaks stay at the same place in the whole domain ($E_0^{\rm th}$; $E_0^{\rm sc}$) a very slow drift is observed in the dynamical regime for the 35-peak and filled patterns. It is of order $0.03\lambda_{\rm th}$, per thousand of round-trip time. Studying the drift would require an extremely large computing time. Nevertheless an interesting observation must be reported. In the 35-peak pattern most of the peaks (those which have close neighbors) drift, but a few peaks having more distant neighbors stay in place. In conclusion, we observe that chaotic localized structures with sufficiently isolated peaks are temporally more stable and more coherent than the filled structure.

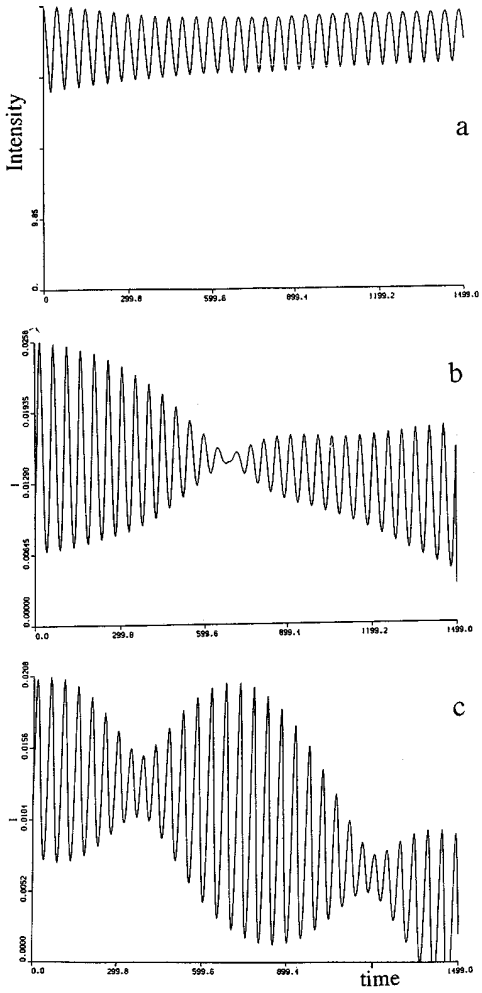

FIG. 4. Intensity time trace for the filled structure at three different points of the grid, vs time, for $E_0=0.0098$. The time interval is equal to $1500d$. With grid dimensions between -1 and $+1$, the traces are (a) at the center $I(0,0,t)$, (b) $I(0.67,0.2,t)-0.0455$, and (c) $I(-0.81,-0.59,t)-0.0455$. The decrease in traces (b) and (c) is due to the slow motion of the peaks, discussed in the text.

III. COMPARISON WITH THE (L-L)MODEL

At this stage it is necessary to understand why, for the present study of 2D localized structures, the delay model (1) cannot be reduced to the well-known Lugiato and Lefever (LL) model [12] for the passive ring cavity in the dispersive limit,

$$\frac{dE}{dt'}=E_0'-E+i(\beta'|E|^2-\theta)E+i\nabla_T^2E, \tag{5}$$

which also displays localized structures at nascent optical bistability [6,7]. In Eq. (5), the time is scaled to the photon lifetime in the ''dressed'' cavity $t_{\rm ph}=d/(1-\rho')$, the transverse variables in Eq. (1) have been rescaled as $\sqrt{a(L/2k)}x\rightarrow x$, and

$$\beta'=a\frac{\alpha\ell\Delta}{2},\quad a=\frac{\rho'}{1-\rho'} \tag{6}$$

with $\rho'=\rho e^{-\alpha\ell/2}$.

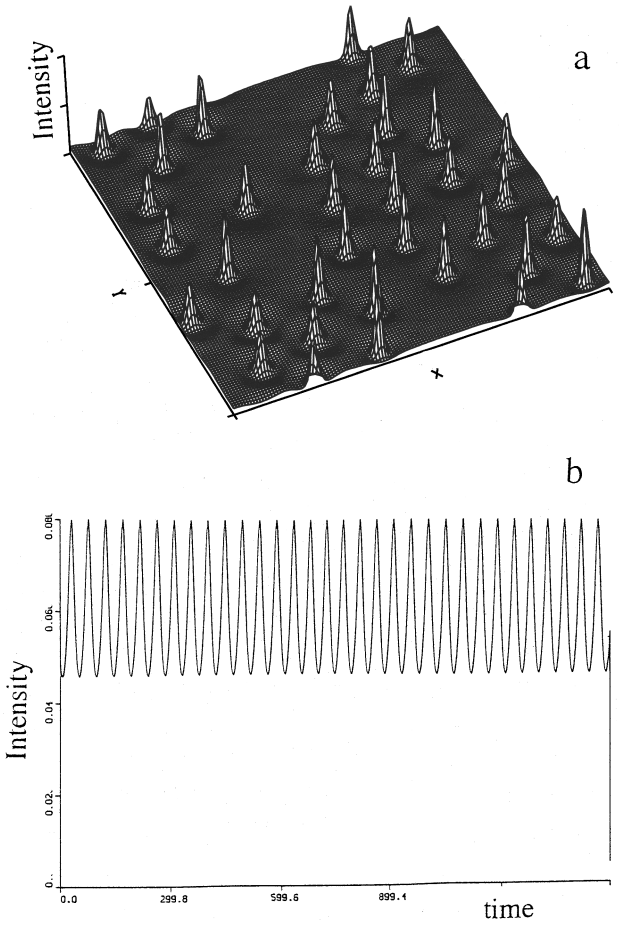

FIG. 5. (a) 3D graph of the intensity $I(x,y)$ for the 35-peak structure, at $E_0=0.01$. (b) The intensity time trace of the ''isolated'' peak located at $(-0.375$ and $0.24)$. This peak does not move during the recording time equal to $1500d$.

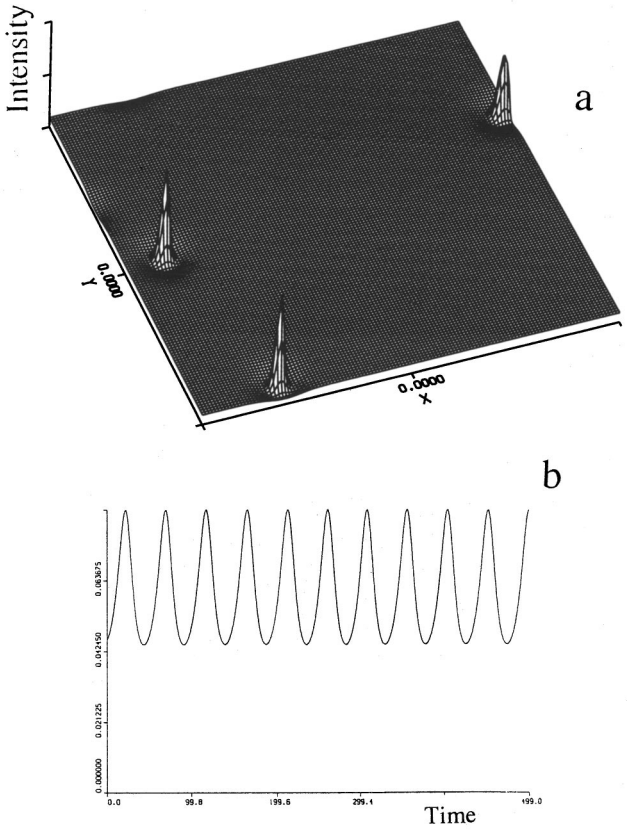

FIG. 6. (a) 3D graph of the intensity $I(x,y)$ for the three-peak structure. (b) The intensity time trace of any peak, at $E_0=0.01$.

The equivalence of Eqs. (1) and (5) is questioned because, in a certain range of parameters the envelope Eq. (5) is a fairly good model of the delay equations (1). For example, the equivalence occurs at the onset of instability in the case of a tuned cavity ($\theta=0$). Static hexagons are found for both models, on the focusing side of the resonance [7,9]. Moreover the biconical square pattern observed with Eqs. (1) on the defocusing side of the resonance was analyzed [10] by using a generalized version of the LL model including the multiconical process ($\nabla_T^2 E \rightarrow \sin\nabla_T^2 E$). The originality of the present work lies precisely in the presentation of 2D localized structures for an equation valid in a larger domain than the envelope equation (5); thus we present the differences between the two models.

A necessary condition for any model equation to reproduce the main features of the original system of equations is that the threshold characteristics displayed by the linear stability analysis are the same. The result of the linear stability analysis of the stationary solution shown in Fig. 7 for Eqs. (1) and (5) is schematized in Figs. 1 and 8, respectively. First we note that if the parameter a, which is equal to 9 [Eq. (2)], is slightly increased by an amount of 10% in the scaling of the horizontal axis, the static boundaries of Figs. 1 and 8 agree very well with the minimum at $\beta'|E_{\rm th}|^2=1$ and $aK_{\rm th}^2+\theta=2$. The small discrepancy is easily explained by the first-order truncature performed in the expansion of the exponential of Eqs. (1). Second the delay model displays a dynamical instability boundary, while the LL model only displays a static boundary. Indeed the LL model amounts to writing $E(t+d)=E(t)+d(dE/dt)$ in Eq. (1) which leads to a linear problem with two eigenvalues only, while the delay model has a dispersion relation which is not polynomial, with many solutions. Nevertheless one can assert that the two models should agree in the limit of small intensity, or more precisely if

$$\tfrac{1}{2}\alpha\diagup\Delta|E|^2\ll 1 \tag{7a}$$

or

$$r=\beta'|E|^2\ll a. \tag{7b}$$

For example, the two models agree for a mistuning θ close to the value $\sqrt{3}$, in the 1D case. Indeed the inhomogeneous 1D solutions of Eq. (5) display ''small'' peak intensity, with $r\approx 2$ as reported in Fig. 11 of Refs. [6,7]. Therefore the 1D localized structures studied by Tlidli and coworkers are also solutions of Eqs. (1), and shall not be reported here.

The 2D structures behave differently. A simple explanation can be obtained from the weakly nonlinear analysis. Above threshold, for $I=I_{\rm th}+\delta I$, the bandwidth δK of the unstable wave numbers may contain a larger number of active modes in two dimensions than in one dimension. Indeed, with a quadratic nonlinearity, the first-order nonlinear term

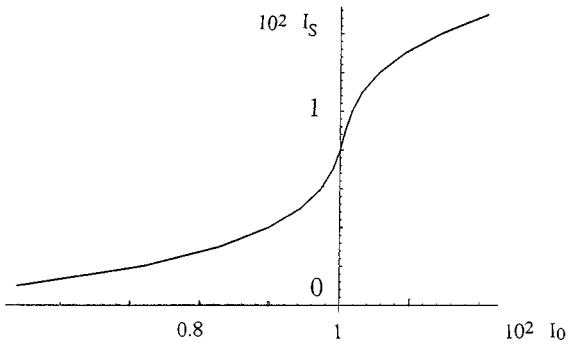

FIG. 7. Plane-wave stationary solution of Eqs. (1) for the intensity I_s vs the input field amplitude E_0.

involved in a 2D pattern with two active wave vectors $\mathbf{K}_i$ and $\mathbf{K}_j$ has components at $\mathbf{K}_i \pm \mathbf{K}_j$, which have more chance of belonging to the unstable band, and then becoming active, than the component $2\mathbf{K}$ which is the only nonlinear component in the 1D case.

The structure at threshold displayed a weakly chaotic time trace with a mean period about 50 d, which qualitatively agrees with the linear analysis predictions. We also performed numerical simulations in the case of instantaneous atomic response, $T_1=0$, and found similar results, i.e., localized structures with high-intensity peaks and weakly chaotic time traces of long period, $T\approx 65$ d, while the dynamical boundary is too high to be invoked in the process.

In conclusion, the chaotic solutions observed with the delay model of the ring cavity, for $T_1=0$, and $T_1=d$, are attributed to the interplay of a broadband of wave numbers active near nascent bistability, which leads to spatial chaos with large intensity modulations.

IV. FROM DISORDER TO ORDERING

Why does the hexagonal order setup for a quasituned cavity ($\theta_{\rm cav}<0.1$) disappear for higher values of the cavity mistuning? What happens near the critical point $\theta_{\rm cav,ob}=0.17$? At nascent bistability, the lowest boundary in Figs. 1 and 8 is quasitangent to the ordinate axis ($K=0$). Therefore one can expect that a large range of wave numbers located near the minimum become unstable. Note that in the case studied here the homogeneous solutions does not display bistability (cf. Fig. 7).

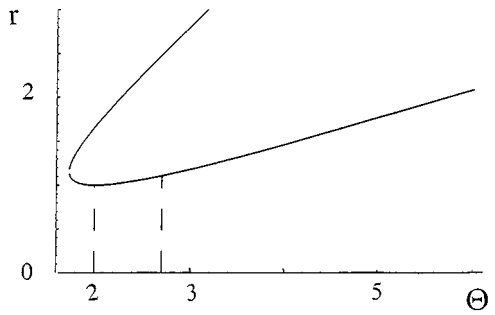

FIG. 8. The marginal stability curve for Eq. (5), r vs Θ, the position of the vertical axis corresponds to $\theta=1.6$. The two dashed lines are located at abscissa corresponding to $K_{\rm th}$ and $\sqrt{3}K_{\rm th}$.

The derivation of an amplitude equation for an ordered structure with a single wave number K_c is questionable, since an analytical description of the pattern formation has to take into account the whole domain near the minimum. That was done for the case of the ring cavity in the absorptive limit [13]. The normal form of the original equations was shown to be a Swift-Hohenberg equation. The derivation of a normal form shows some generic properties, but one finally has to solve a partial differential equation.

In this section we try to investigate the chaos in another way. We propose to control the formation of chaotic structures appearing in the vicinity of nascent optical bistability, by reducing the wave-number bandwidth by a low-frequency filtering procedure that eliminates all the wave numbers larger than a given value K_f. An appropriate filter allows us to obtain stationary ordered solutions with ''small'' amplitudes of modulations. Therefore we derive the properties of the filtered solution from a weakly nonlinear analysis of the LL model. In Secs. IV A and IV B, the role of the filter is first analytically investigated, then numerical results are presented.

A. Amplitude equation for the hexagons

With $E=E_s(1+\mathcal{A})$, the LL model (5) becomes

$$\partial_{t'}\mathcal{A}=-\mathcal{A}+i\,r(2.\mathcal{A}+\mathcal{A}^*+\mathcal{A}^2+2|.\mathcal{A}|^2+\mathcal{A}|.\mathcal{A}|^2)+i(\nabla_T^2-\theta).\mathcal{A}, \tag{8}$$

The amplitude equation for a hexagonal pattern with a critical wave number $K_{\rm th}$ was already given in Refs. [7,9], and generalized in Ref. [11] for an arbitrary wave number K_c near critical value $K_{\rm th}$. Here we recall the results with the notations of Ref. [11]. At first order, the complex amplitude of the electric field $\mathcal{A}_1=R_1+iI_1$ has real and imaginary parts

$$R_1=A_1e^{i\mathbf{K}_i\mathbf{x}}+B_1e^{i\mathbf{K}_j\mathbf{x}}+C_1e^{i\mathbf{K}_m\mathbf{x}}+\text{c.c.}, \tag{9}$$

$$I_1=cR_1, \tag{10}$$

where $\mathbf{K}_{i,j,m}$ are three wave vectors with vertex angles $\pi/3$ and equal moduli K_c. In Eq. (10), the parameter c depends on the wave number K_c via the relation

$$c=-\Theta+3r_c \tag{11}$$

in the focusing case, $\Theta=K_c^2+\theta$,and $r_c(\Theta)$, drawn in Fig. 8, is expressed as

$$r_c=(2\Theta\pm\sqrt{\Theta^2-3})/3. \tag{12}$$

The filtering procedure amounts to canceling all the components with wave vector $K\geqslant K_f$ of the second-order solution

$$R_2=\alpha_0(R_1^2)_0+\alpha_1(R_1^2)_K+\alpha_3(R_1^2)\sqrt{3}K+\alpha_4(R_1^2)_{2K}, \tag{13}$$

where the index in (R_1^2) is relative to the modulus of the wave vector, and

$$\alpha_1=cr_c/2, \tag{14}$$

$$\alpha_n=\frac{f_2(n)+b(n)g_2(n)}{b(n)c(n)-1} \qquad \text{for } n\neq 1, \tag{15}$$

with $b(n)=\Theta_n-r_c$, $c(n)=3r_c-\Theta_n$, $\Theta_n=nK^2+\theta$, $f_2(n)=2r_c c(n)(R_1^2)_n$, and $g_2(n)=-(3+c^2)r_c(R_1^2)_n$.

The amplitude equations for the subcritical hexagons $A=\varepsilon A_1=B=C$ reduce to

$$\partial_\tau A=\mu A+2(1+\ell\mu)A^2+(e+2f)A^3, \tag{16}$$

where $\mu=(r-r_c)/r_c$, and

$$e=2\alpha_0+\alpha_4+3j, \quad f=2(\alpha_0+\alpha_1+\alpha_3+3j), \tag{17}$$

$$\ell=1-\frac{3+c^2}{3-c^2}\alpha_1, \quad j=\frac{1-c^4}{3-c^2}. \tag{18}$$

1. Without filter

Let us describe first the amplitude diagrams $A(\mu,K_c,\theta)$ in the usual case, when all the components K_c, $\sqrt{3}K_c$, and $2K_c$ are allowed to interplay for the pattern formation (no filtering). For a critical wave number $K_c=K_{\rm th}$, it is already known [7,9] that $A(\mu)$ become larger and larger values as the cavity mistuning increases from $\theta=0$ to $\theta\approx 1$, and that the third-order Landau expansion [Eq. (16)] has no solution for $\theta>1$. Actually reasonable values for A lies *below unity* since a hexagonal pattern with maxima of intensity of order ten times the homogeneous solution corresponds to $A\approx 0.7$. We shall now investigate the behavior of the solution of Eq. (16) for $K_c\neq K_{\rm th}$.

In the domain $0<\theta<1$, where Landau expansion is valid for $K=K_{\rm th}$, the amplitude drastically increases with K, as shown in the 3D graph [Fig. 9(a)], which displays the threshold amplitude $A_0=A(\mu=0)=-2/(e+2f)$ in the parameter space $(\Theta=K^2+\theta,\theta)$. For example, for a tuned cavity the amplitude diagram reported in Fig. 9(b), for three values of the wave number close to the critical one $K_{\rm th}$ diverges at $K\approx 1.2K_{\rm th}$. Does this predict that hexagons will appear with a wave number larger than $K_{\rm th}$? This would disagree with the numerical results, which display hexagons with the critical wave number $K_{\rm th}$ for $\theta=0$.

The same observation was done for the case $\theta=0.7$, studied by Tlidli: the numerical hexagons were found with K_c slightly smaller than $K_{\rm th}$, while the amplitude is also an increasing function of K [Fig. 9(c)]. In both cases the numerical results agree with the analytical predictions in the domain $K\approx K_{\rm th}$ only, where the weakly nonlinear analysis is valid. For $K>K_{\rm th}$, the dramatic growing of the amplitude predicted by the Landau expansion is meaningless, and does not lead to a shift of the critical wave number (called the ''nonlinear resonance'' effect in Ref. [16]).

2. Amplitude diagram with filter

Now let us describe the amplitude diagrams obtained by canceling the components with wave numbers larger than K_c. The 3D graph $A(\mu=0,\Theta,\theta)$ in Fig. 10(a) displays strong differences from the graph in Fig. 9(a). In particular, for small detuning, $0\leqslant\theta\leqslant 1$, the filtering procedure suppresses the divergence of the solution of Eq. (16), and in the domain $\theta>1.4$ only Eq. (16) ''with filter'' has a solution, as

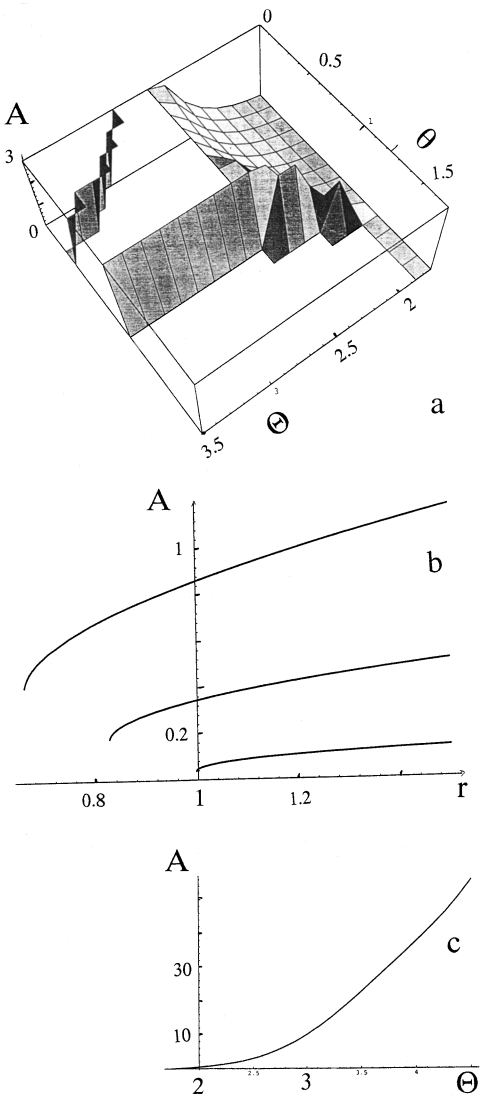

FIG. 9. (a) 3D graph of the threshold value of the amplitude $A(\mu=0,\ \theta,$ and $\Theta)$ for one hexagonal component, without any filter, vs the cavity mistuning $0<\theta<\sqrt{3}$ and the diffraction parameter $\sqrt{3}<\Theta<3.5$. (b) Amplitude diagram $A(\mu,\theta=0,\Theta_i)$, for three values of the diffraction parameter $\Theta_i=1.9$, 2, and 2.2. The amplitude increases with Θ, and diverges at $\Theta=2.8$. (c) Amplitude $A(r=1.2,\ \theta=0.7,\ \Theta)$ for a given value of the control parameter $r=1.2$, and mistuning $\theta=0.7$.

expected. Let us focus on this domain, which is close to nascent optical bistability. The solution of Eq. (16) exists for a certain range of wave-number values only, as illustrated in Figs. 11(a)–11(c), where the value of the amplitude $A(r=1.2)$ is reported as a function of the diffraction parameter $\Theta=K^2+\theta$, for the three values of mistuning $\theta=1.4$, 1.5, and 1.6. As one approaches the bistability, the domain of existence of a solution shrinks. The right part of the curves in Figs. 11 are meaningless for a low-frequency filtering, and will not be considered.

For $\theta=1.6$, in the left part of the curve, amplitude A is smaller than unity in a very small domain, for a wave number smaller than $K_{\rm th}$ only (or Θ smaller than 2), as shown in Fig. 10(b). But for $\theta=1.4$, the amplitude A is smaller than unity in a larger domain, for $K\leqslant 2K_{\rm th}$. In this region the amplitude slowly increases, then hexagons are expected to

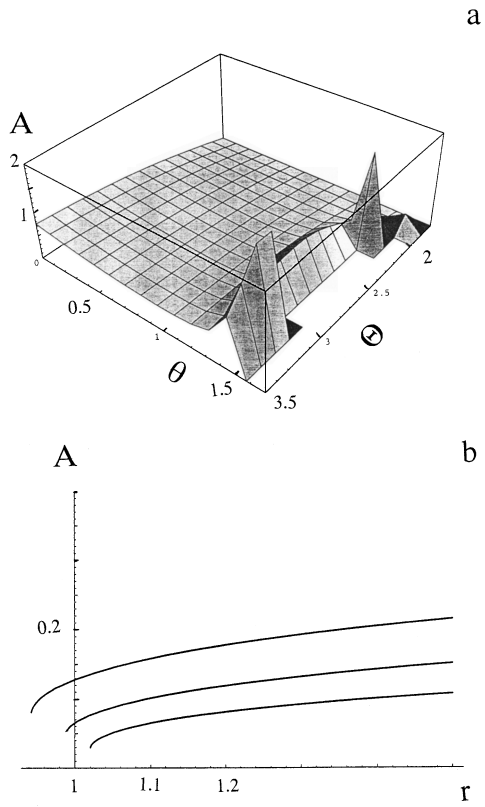

FIG. 10. (a) 3D graph of the threshold value of the amplitude $A(\mu=0,\ \theta,$ and $\Theta)$ for one hexagonal component, with a filter cutting the $\sqrt{3}$K and 2K components, vs the cavity mistuning $0<\theta<\sqrt{3}$ and the diffraction parameter $\sqrt{3}<\Theta<3.5$. (b) Amplitude diagram $A(\mu,\theta=1.6,\Theta_i)$, for three values of the diffraction parameter $\Theta_i=1.78$, 1.8, and 1.82. The amplitude increases with Θ, and diverges at $\Theta\approx1.9$.

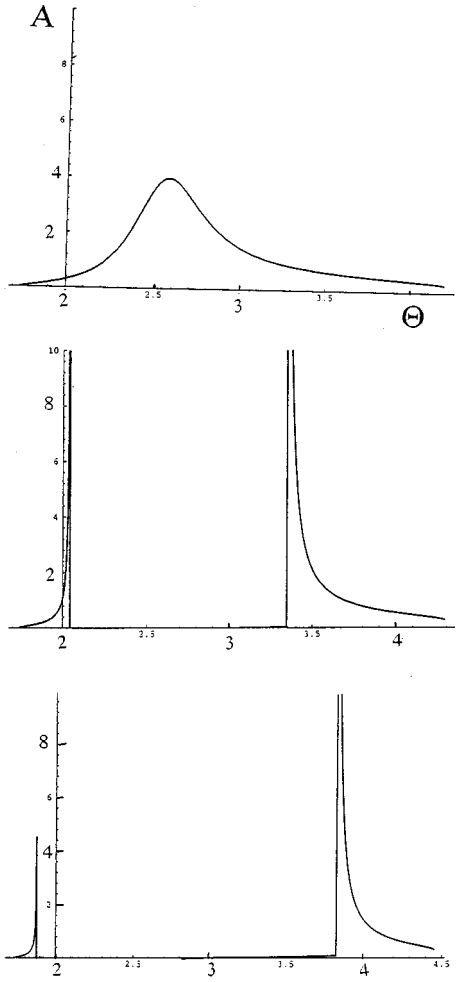

FIG. 11. Amplitude $A(r=1.2,\ \theta_i,$ and $\Theta)$ with the filter, as in Fig. 10, for three values of the cavity mistuning $\theta_i=1.4$, 1.5, and 1.6, from top to bottom, vs the diffraction parameter Θ.

appear with wave numbers larger than the critical one.

B. Numerical results

What about the numerical simulations of Eqs. (1) with a filter? In the numerics the K_f filter is easily introduced in the code using a fast Fourier transform for the propagation in the free space of the cavity [Eq. (1a)]. The mistuning is the same as in the Sec. III, $\theta_{\rm cav}=1.6$, that corresponds to $\theta\approx1.6$, within 10% of uncertainty due to the shift in the parameter a for fitting the marginal curves of both models [Eqs. (1) and (5)].

1. Circular filter

The cutoff K_f increased progressively from $K_{\rm th}$. When K_f is slightly larger than $K_{\rm th}$, a hexagonal pattern is obtained (Fig. 12). The wavelength is nearly equal to the critical one. The peak intensity is not larger than twice the stationary value I_s, that corresponds to a small amplitude, $A\approx0.1$, as in the diagrams of Fig. 10(b). In this regime relations (7) are fulfilled and then the LL model approximates Eqs. (1). As K_f increases until 1.5 $K_{\rm th}$ $(2<\Theta<2.4)$, the pattern remains hexagonal, with an increasing maximum intensity $2<3$ still fulfilling the equivalence relation (7), that corresponds to small modal amplitude $0.1<A<0.2$. The striking observation concerns the shift in the spatial frequency, the wave number of the hexagons increasing with K_f, keeping a value close to K_f. More precisely, one observes that the critical wave number is *shifted* from $K_{\rm th}$ to $1.4K_{\rm th}$ (or the diffraction parameter is shifted from $\Theta_c\approx2$ up to 2.4). The observation of small amplitude hexagons in this domain qualitatively agrees with the analytical curve shown in Fig. 11(a), corresponding to $\theta=1.4$, which displays the so-called ''nonlinear resonance effect'' [16].

The hexagons are stable up to 20% above threshold. Moreover they are also obtained with an hypergaussian input beam, in the same range of control parameter.

When $K_f\approx1.7K_{\rm th}$, the pattern becomes a bisquare (Fig. 12), with two critical wave numbers close to K_f and $(1/\sqrt{2})K_f(\Theta_c\approx1.17$ and 2.75). For a filter with a broader bandwidth, the disorder appears (see also Fig. 2).

2. Square filter

A square filter is transparent in the domain $\{|K_x|<K_f$ and $|K_y|<K_f\}$. The pattern obtained near the threshold is also a bisquare when the cutoff is close to the critical wave number $K_{\rm th}<K_f<1.3K_{\rm th}$. The preferential square structure (with respect to the hexagonal one obtained with a circular filter) results from the use of a square filter, which allows the growing of wave vectors with the resonant $\mathbf{K}_x\pm\mathbf{K}_y$ components.

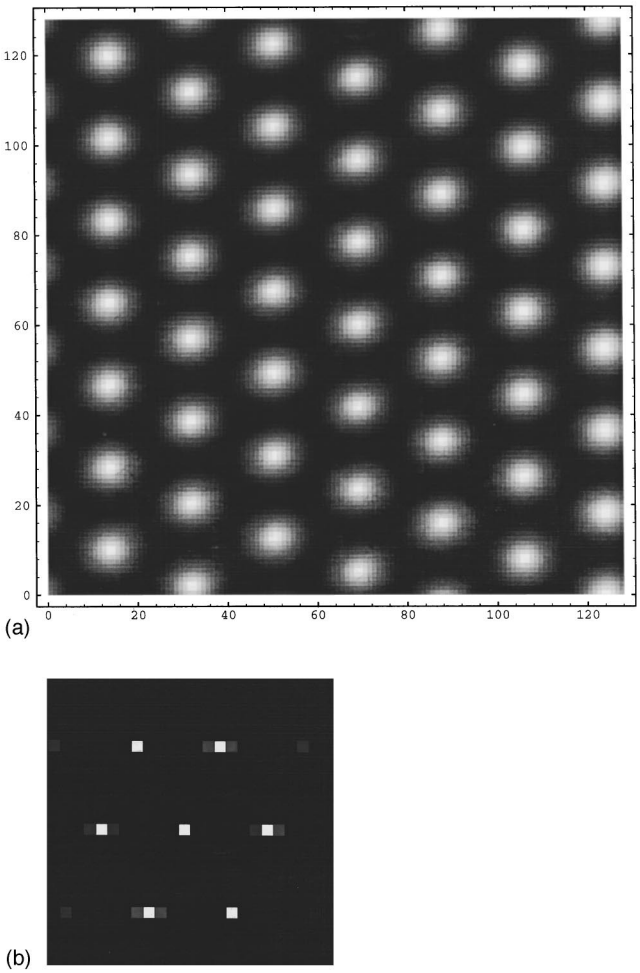

FIG. 12. Hexagonal pattern obtained at $\theta_{\mathrm{cav}}=0.16$ and $E_0=0.0105$, with a circular filter with K_f slightly larger than K_{th}. (a) Near field intensity. (b) Far-field intensity.

But when the cutoff is $K_{x,yf}\approx 1.2K_{\mathrm{th}}$, the bisquare is obtained whatever the shape of the filter. Finally, as soon as the intermodal $K-\sqrt{2}K$ coupling is allowed, the chaotic solution is changed into a square pattern.

Let us recall that on the defocusing side of the resonance, the solution of Eqs. (1) also displays a bisquare pattern, which results from the emission of two critical wave numbers with a ratio close to the magic value $\sqrt{2}$, belonging to the first and second near-axis instability domains, respectively. In the case observed here, the filtered solution has two wave numbers belonging to the first instability domain (Fig. 8). What differs in the biconical and monoconical bisquares? As shown in the analytical treatment of the bisquare pattern performed in Ref. [11], the relevant parameters for a multimodal interaction are not the set of wave numbers K_n for the different active modes, but the set of associated diffraction parameters $\Theta_n=a\ \sin[(LK_n^2/2k)+\eta\theta]$. In other words, the predictions for a bisquare with diffraction parameters Θ_1 and Θ_2 are identical for a biconical or monoconical emission. We showed in Ref. [11] that, in the defocusing case, the pattern spontaneously emerging from noise is a bisquare with $K_2=\sqrt{2}K_1$ when two sets of active modes with $\Theta_2=2\Theta_1$ are allowed to interplay. Here we show that the hexagons, disappear in favor of a bisquare pattern in the focusing case, for the set ($\Theta_1=2.2$, $\Theta_2=2.75$).

In conclusion, we propose a very simple procedure to change the disorder into either a hexagonal or a bisquare ordered solution. A low-pass filter which cuts a portion of the spatial frequencies allows the chaotic solution, obtained at the onset of instability and close to the nascent optical bistability, to recover the order corresponding to a tuned cavity. When the wave-number bandwidth is large enough to allow the K-$\sqrt{2}K$ interaction, the pattern is a bisquare as in the defocusing case, and with a narrow filter the pattern is hexagonal as in the focusing case.

V. DISCUSSION

The present work is purely numerical, but the parameter values are those of the feedback mirror device [17], where transverse instabilities were first observed in optics. The ring cavity set up was chosen in our numerical work, because the dynamical properties of the instabilities were shown to be described within the adiabatic approximation (elimination of the polarization) [10], while the ''$2d$'' oscillation of the feedback mirror experiment is not explained within this frame [18], as written in Sec. II. In the latter experiment the nonlinear medium was a weakly absorptive and strongly dispersive cell containing sodium atoms with a buffer gas. A laser beam was sent through the medium and reflected back to the cell via a quasiconfocal mirror. The optical arrangement was chosen to be a half-cavity, preferentially to a ring cavity, in order to get rid of fluctuations of the laser frequency over a time interval much larger than the round-trip time d. The problem of stability of the cavity mistuning over many round-trip times seems to be passed over now [19]; thus an experiment in a ring cavity with two-level atoms could be done.

The conditions for the existence of localized structures is still an open question. As noted in Ref. [8], the whole class of partial differential equations that have localized solutions is not yet known. A necessary condition for the appearance of localized structures is the existence of a subcritical bifurcation, since in this case two stable solutions may coexist. However, this condition is not sufficient. For example, subcritical hexagons are often observed without coexistence of localized solutions. A condition that favors the existence of localized structure in two dimensions is that they also exist in one dimension [1,5,7]. In other words, a necessary condition for the existence of 2D localized structures seems to be the subcriticallity of rolls, and also of the observed 2D pattern if it differs from rolls. This double subcriticality occurs here.

While the existence of 2D localized structures is connected to the existence of 1D structures, the present work shows that the solutions may be very different in one and two dimensions. The 1D solution of Eqs. (1) is stationary, with a ''small'' modulation of the homogeneous intensity, and maxima of intensity located close to the first static boundary in Fig. 1, while the 2D solution displays large intensity peaks resulting from the richness of the intermodal coupling in two dimensions, near nascent optical bistability. The present work enlarges the family of localized structures to cases where the stable homogeneous solution is connected, not to a stable homogeneous or inhomogeneous or-

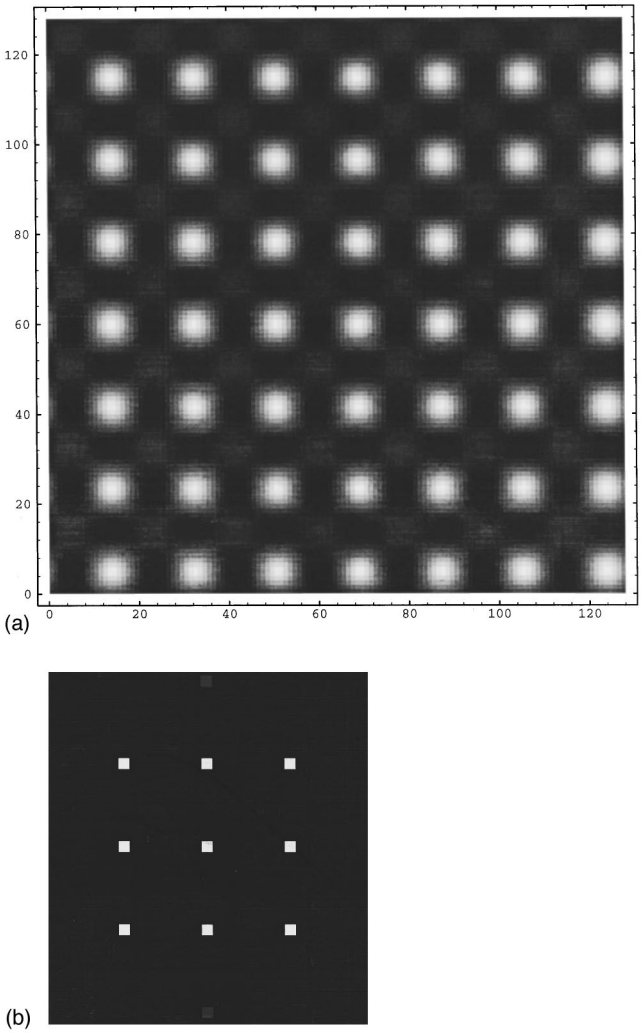

FIG. 13. Bisquare pattern obtained at $\theta_{cav}=0.16$, and $E_0=0.0105$, with a circular filter with $K_f \approx 1.7K_{th}$. (a) Near-field intensity. (b) Far-field intensity.

dered solution, but to spatiotemporal chaos.

The solitons [20] and the solitary waves [21,22] are sometimes referred to as belonging to the same family as the localized structures. They do, in the sense that they are often defined as solutions which connect two stable coexisting states. But we must emphasize some important differences. As described here, the localized structures appear spontaneously on the transverse profile of a plane-wave input beam, when decreasing the control parameter below the onset of the ''filled'' structure. As studied in Ref. [4], a front connecting the inhomogeneous and homogeneous states propagates in the transient, then the front velocity vanishes because of pinning between the front and the flat structure. Differently from the localized structures are the stationary solutions formed with a finite-size beam, which makes the solution vanish at a finite distance from the optical axis. As an example, let us quote the stationary solitary waves obtained with Eqs. (1) for $\theta=0$, with a finite-size input beam. In this case (tuned cavity), no localized solution is found with a plane-wave input. The solitary waves obtained with a circular input look like daisy patterns with 1–15 petals distributed on one or two circles at the top of the exit profile. If one or several petals are removed, and the truncated daisy is used as the initial condition, the full daisy pattern quickly forms. Increasing the size of the circular input changes the daisy into a filled hexagonal structure.

What are the processes stabilizing the localized solutions in our system? As argued in Ref. [23], the stability of the solutions may result from a nonvariational effect, since our system is dissipative and dispersive. (However, stable localized structures have also been observed in numerical simulation of the variational Swift-Hohenberg equation [5].

Another stabilization process, which was invoked by Coullet and Emilson [1], is resonant forcing. The ''bubble'' observed in Ref. [1] was attributed to the stabilizing effect of a strong forcing close to twice the natural frequency of the oscillators. In passive systems, the forcing is due to the input beam. It corresponds to the term E_0 in Eq. (1b), and has the natural frequency of the ''oscillators''. Without this term the unique stationary solution is the trivial one, and no instability can be built up. Thus the resonant forcing has here a destabilizing effect, necessary to balance the strong losses, differently from the Ginzburg-Landau case treated in Ref. [1].

Finally, the filtering procedure, proposed here to ''control'' the spatiotemporal chaotic solution and change it into a stable ordered one, is a very simple and successful method. Recall that a ''period proportional feedback'' method [23] was also successfully applied to control the chaos in multitransverse mode lasers [24].

ACKNOWLEDGMENTS

The numerical simulations were realized with the Cray C98 of the IDRIS CNRS computer center. The authors greatly acknowledge fruitful discussions with T. Erneux, P. Mandel, and M. Tlidli.

[1] P. Coullet and K. Emilson, Physica A **188**, 190 (1992).
[2] A. V. Gaponov-Grekhov, A. S. Lomov, G. V. Osipov, and M. I. Rabinovitch, in *Nonlinear Waves*, edited by A. V. Gaponov-Grekhov, M. I. Rabinovitch, and J. Engelbrecht (Springer, Heidelberg, 1989), Vol. 1, p. 65.
[3] O. Jensen, V. O. Pannbacker, G. Dewel, and P. Brockmans, Phys. Lett. A **179**, 91 (1993).
[4] O. Jensen, V. O. Pannbacker, E. Mosekilde, G. Dewel, and P. Borckmans, Phys. Rev. E **50**, 736 (1994).
[5] M. Tlidli and P. Mandel, Chaos Solitons Fractals **4**, 1475 (1994).
[6] M. Tlidli, P. Mandel, and R. Lefever, Phys. Rev. Lett. **73**, 640 (1994); see also M. Tlidli, thesis, Universite Libre de Bruxelles, Belgium, 1995, and references therein.
[7] A. J. Scroggie, W. J. Firth, G. S. McDonald, M. Tlidli, R. Lefever, and L. A. Lugiato, Chaos Solitons Fractals **4**, 1323 (1994).
[8] H. Brand and R. J. Deissler, Physica A **204**, 87 (1994).

[9] M. LeBerre, S. Patrascu, E. Ressayre, A. Tallet, and N. I. Zheleznykh, Chaos Solitons Fractals **4**, 1389 (1994). See also A. S. Patrascu, Ph.D. thesis, Universite de Paris-Sud, Orsay, France, 1995.

[10] M. Le Berre, S. Patrascu, E. Ressayre, and A. Tallet, Opt. Commun. **123**, 810 (1996).

[11] M. Le Berre, D. Leduc, E. Ressayre, and A. Tallet, Phys. Rev. A **54**, 3428 (1996).

[12] L. A. Lugiato and R. Lefever, Phys. Rev. Lett. **58**, 2209 (1987); L. A. Lugiato and C. Oldano, Phys. Rev. A **37**, 3896 (1988).

[13] P. Mandel, M. Georgiou, and T. Erneux, Phys. Rev. A **47**, 4277 (1993).

[14] K. Ikeda, Opt. Commun. **30**, 257 (1979).

[15] M. Tlidli, R. Lefever, and P. Mandel, Quantum Opt. **8**, 931 (1996).

[16] G. J. de Valcarcel, K. Staliunas, E. Roldan, and V. J. Sanchez-Morcillo, Phys. Rev. A **54**, 1609 (1996).

[17] G. Giusfredi, J. F. Valley, R. Pon, G. Khitrova, and H. M. Gibbs, J. Opt. Soc. Am. B **5**, 1181 (1988).

[18] M. Le Berre, E. Ressayre, and A. Tallet, Phys. Rev. A **43**, 6345 (1991).

[19] K. Staliunas, M. F. H. Tarroja, G. Slekys, and C. O. Weiss, Phys. Rev. A **51**, 4140 (1995); see also the scheme proposed to measure the cavity length by G. Steinmeyer, D. Jaspert, and F. Mitschke, Opt. Commun. **104**, 379 (1994).

[20] A. C. Newell, *Solitons in Mathematics and Physics* (Society for Industrial and Applied Mathematics, Philadelphia, 1985); A. C. Newell, and J. V. Moloney, *Nonlinear Optics* (Addison-Wesley, Redwood City, CA, 1992).

[21] D. W. McLaughlin, J. V. Moloney, and A. C. Newell, Phys. Rev. Lett. **51**, 75 (1983).

[22] N. N. Rosanov, V. A. Smirnov, and N. V. Vyssotina, Chaos Solitons Fractals **41**, 767 (1994), and references therein.

[23] O. Thual and S. Fauve, J. Phys. (France) **4**, 1829 (1988).

[24] R. Martin, A. J. Kent, G. D'Alessandro, and G.-L. Oppo, Opt. Commun. **127**, 161 (1996).